MSc in Photonics

Universitat Politècnica de Catalunya (UPC)
Universitat Autònoma de Barcelona (UAB)
Universitat de Barcelona (UB)
Institut de Ciències Fotòniques (ICFO)

PHOTONICS**BCN**

http://www.photonicsbcn.eu

Master in Photonics

MASTER THESIS WORK

Synchronization of interacting pairs of Silicon-based optomechanical crystals

Elisenda Vitrià Montero

Supervised by Dr./Prof. Daniel Navarro Urrios (UB)

Presented on date 19th July 2022

Registered at

Escola Tècnica Superior d'Enginyeria de Telecomunicació de Barcelona

Synchronization of interacting pairs of Silicon-based optomechanical crystals

Elisenda Vitrià Montero
Departament d'Enginyeria Electrònica i Biomèdica, Universitat de Barcelona, Martí i Franquès 1, 08028 Barcelona
July 2022

E-mail: e.vitria6@gmail.com

Abstract. The coupling between optical and mechanical waves within optical resonators has become a growing study field in the last years due to its scientific and technological importance. Optomechanical crystals (OMCs) are a means not only to achieve this interaction but to create coherent phonon sources required in many applications. This work aims for the synchronization of two OMCs acting as OM oscillators using light as the main coupling mechanism. A characterization of their experimental properties and dynamics is presented, as well as the mechanism to achieve frequency locking when they are brought to the "phonon lasing" regime. Although synchronization is confirmed in the frequency domain, an improved set of OMC samples is needed to obtain a more efficient process.

Keywords: cavity optomechanics, phonon lasing, synchronization.

1. Introduction

Given the absence of discrete phonon transitions in solids at ambient conditions, many technologies have sought the coherent creation of vibration sources, which can be exploited in several applications including on-chip metrology, time-keeping, or force/mass sensing. With this aim in mind, OMCs provide an efficient way to generate self-sustained coherent phonons from tens of MHz to GHz frequencies, typically achieved by using an optical pumping mechanism, the most common being the radiation pressure inside a resonator. In order to successfully achieve the "phonon lasing" regime, modes with high-quality factors and large optomechanical coupling strength are required.

Additionally, phonons can be used as interfaces in communication environments since they can be effectively coupled to other information carriers such as electrons and photons. These applications demand further functions besides the coherent emission of phonons, one of them being the synchronization of different sources. OMCs are also a means to tackle

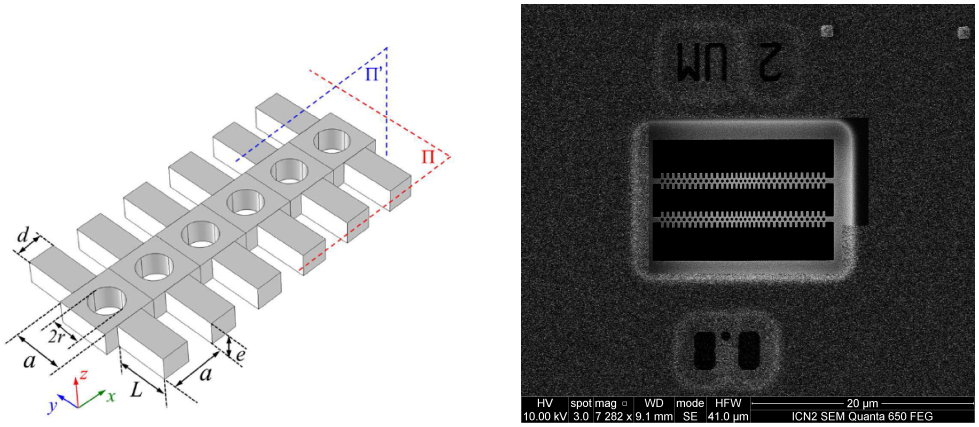

(a) (b)

Figure 1: (a) OMC with its symmetry planes (Π and Π′) and geometry parameters (a, L, d, r, and e). (b) SEM image of the OMC structures composing the sample.

these challenges by the frequency locking between micromechanical oscillators. They can interact via electronic or physical connections. However, interaction through light is the most promising one when it comes to long-distance propagation with minimal loss [1].

1.1. OM cavity

This study is performed in Optomechanical Crystals (OMCs), nanopatterned metamaterials or dielectrics fabricated to control and manipulate the propagation of light and sound. They can exhibit simultaneously photonic and phononic bandgaps, thus allowing the confinement of optical and mechanical modes to form a complete optomechanical system. Crucially, the improvement of the interaction between radiation pressure and matter within such crystals involves effectively trapping both modes within a cavity in order to enhance their coupling. Previous work [2] has concluded that a particular 1D silicon OMC exhibits bandgaps for electromagnetic (in the hundreds of THz) and mechanical (in the GHz) waves. It also supports mechanical string-like modes, which can also display large optomechanical coupling. It is comprised of a straight silicon nanobeam waveguide with parallelepiped stubs attached on both sides and circular holes drilled in the middle, as illustrated in FIG. 1a. Furthermore, it was realized that adding a defect into these crystals by gradually reducing the unit cell parameters from both sides of the waveguide towards the center, leads to high optical Q factors, which are essential to obtain the enhancement of the optomechanical interaction.

Our sample comprises two nanobeams fabricated in a silicon-on-insulator chip with standard nanofabrication techniques, both of which share identical geometric characteristics by design (FIG. 1b). However, due to fabrication imperfections, the eigenfrequencies of the two OMCs are slightly shifted, both in what regards the optical and the mechanical modes. As we will see later on, the latter is a crucial condition since this experiment seeks to synchronize their mechanical dynamics, having them oscillate at the same frequency by means of the so-called Master-Slave configuration.

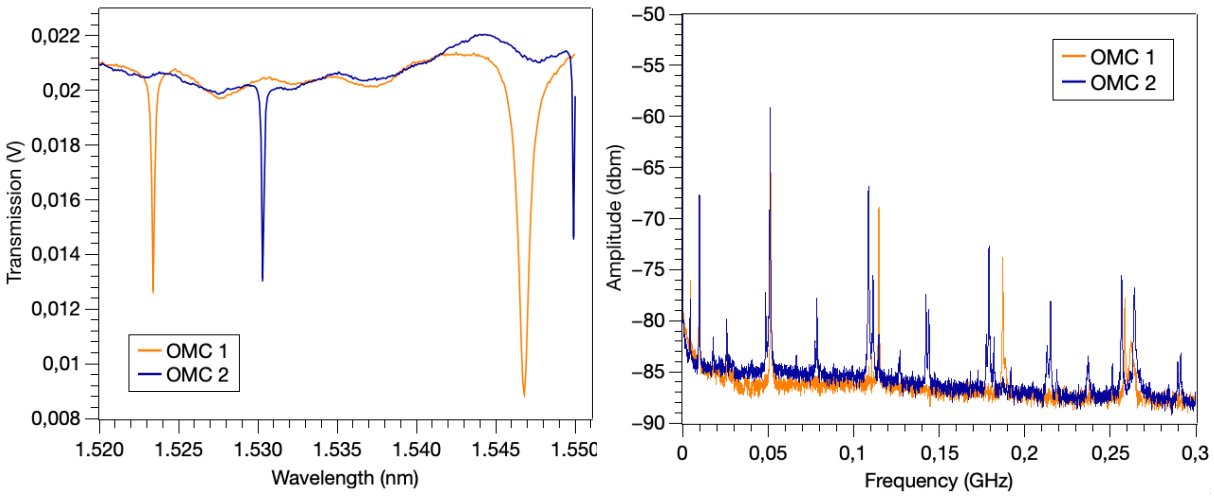

(a) (b)

Figure 2: (a) Transmitted optical signal displaying the first modes of both structures at low input power (0.2mW). (b) RF spectrum displaying the thermally driven low-frequency modes of both OMCs.

1.2. Experimental characterization

In order to characterize the OM structures of our sample, it is necessary to investigate the electromagnetic and mechanical waves that can be confined within both crystals. The experimental setup to perform the characterization uses an IR tunable laser, whose light passes through a polarization controller and is coupled to a tapered microlooped fiber [3]. By positioning the nanobeam near the loop's evanescent field, light is able to enter the cavity and excite a specific optical mode. An IR detector receives the transmitted optical signal conveying non-resonant wavelengths, and finally, the signal reaches the spectrum analyzer, which measures the input's radiofrequency (RF) power spectrum.

With low optical input power, the transmitted signal reveals inverted Lorentzian peaks corresponding to optical resonances, as shown in FIG. 2a. In order to observe the interaction between optical and mechanical waves, the transduction mechanism must be introduced. Essentially, the mechanical motion of the structure moves the photonic resonance at the mechanical eigenfrequencies, thus modulating the transmitted signal. Although all mechanical modes exist in the OMC, only those with a certain degree of OM coupling (g_{OM}) are detected in the RF spectrum. In the low frequency range (tens to hundreds of MHz) we detect the string-like mechanical modes involving the whole OMC geometry. In this range, the modes with large enough g_{OM} to be visible are the in-plane flexural modes with an antinode at the center. FIG. 2b shows the thermally-activated transduced mechanical modes of each OMC by setting the laser within its first optical resonance. Additionally, in order to evaluate the effectiveness of each mode, we calculate its quality factor (Q) from the spectra of optical and RF signals (table 1).

It is pertinent to note that while the first OMC shows relatively higher values than the second one, the most noticeable aspect is the magnitude difference between the optical and mechanical Q-factor values. Room atmospheric conditions and, particularly, friction with

Table 1: Quality factor values for the lower mechanical and optical modes of each cavity.

Q-factor	OMC 1	OMC 2
Optical	7733 (1523 nm)	8645 (1530 nm)
Mechanical	250 (51 MHz)	261 (51 MHz)

the environment are the dominant dissipating mechanism in this frequency range, which accounts for most of the losses for this type of phonons.

2. Nonlinear dynamics of an OMC system

High energies stored in optical resonators can produce considerable nonlinear effects (NL) that are usually not desired in photonic crystals. However, since these optical nonlinearities are able to intercouple with the mechanical modes of a nanobeam and affect the relative detuning between an optical resonance and the excitation laser, they may provide a new way of exploring different dynamics among these crystals.

As stated in [4], in silicon-based OMCs such as those in our sample, two main sources lead to optical nonlinearities: free-carrier dispersion (FCD) and thermo-optic (TO) effect. The former is caused by an excess of free carriers density (N) introduced by two-photon absorption (TPA), thus reducing the material's refractive index. Consequently, the resonant wavelength (λ_r) experiences a blueshift proportional to N as compared to its unperturbed position (λ_0). The TO effect occurs when the average cavity temperature (ΔT) rises, causing the refractive index to increase, and redshifting the resonance position proportionally to ΔT. Therefore, first-order NL effects affect the resonant wavelength as follows:

$$\lambda_r = \lambda_0 - \frac{d\lambda_\mathrm{r}}{dN}N + \frac{d\lambda_\mathrm{r}}{d\Delta\mathrm{T}}\Delta T \tag{1}$$

Considering that free-carrier absorption (FCA) is the main source of heating, both dynamics are interrelated and may be described through a system of coupled rate equations.

$$\dot{N} = -\frac{1}{\tau_\mathrm{FC}}N + \beta\left(\frac{hc^3}{n_r^2\lambda_0 V_0^2}n^2\right) \tag{2}$$

$$\dot{\Delta T} = -\frac{1}{\tau_\mathrm{T}}\Delta T + \alpha_\mathrm{FC}Nn \tag{3}$$

Where β is the TPA tabulated coefficient, n_r the refractive index, and V_0 the optical mode volume. The first term in Eq.(2) represents surface recombination driven by τ_FC, namely the rate at which the temperature increases per photon and unit free-carrier density. In Eq. (3), the heat dissipated to the surroundings of the cavity volume (governed by the characteristic lifetime τ_T) is compensated for by the part of the photons that are absorbed and transformed into heat through FCA. The number of intracavity photons (n) depends on the relative detuning between the laser and the optical resonance and establishes an intercoupling between the two equations. The maximum value of n is reached when the laser wavelength coincides with the resonant wavelength ($\lambda_\mathrm{l} \simeq \lambda_\mathrm{r}$).

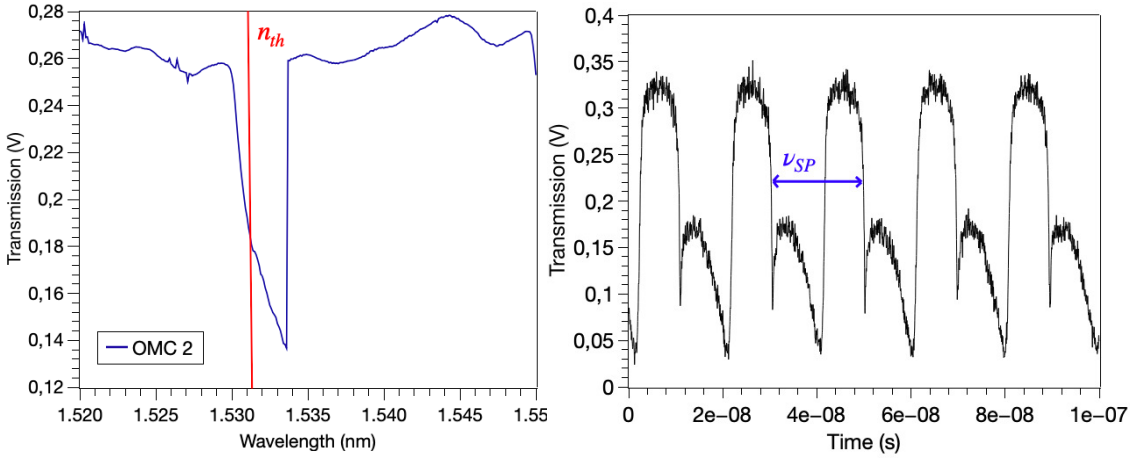

(a) (b)

Figure 3: (a) Transmitted signal at P = 2mW for the OMC 2. (b) Periodic anharmonic variation over time of the transmitted signal during SP regime.

According to FIG. 3a, increasing the optical input power from 0,2 mW to 2 mW redshifts the resonant wavelength due to the TO effect, causing a "saw-tooth" profile instead of a Lorentzian line shape. Initially, when λ_l is close to λ_0, and n is small, the solution of the 2D system $\{\Delta T, N\}$ is a stable fixed point. As the laser-resonance detuning decreases, more light enters the cavity eventually reaching a threshold (n_{th}). At that point, the solution transforms into an unstable fixed point surrounded by a stable limit cycle denoted as Self-Pulsing [6].

2.1. Self-Pulsing (SP)

This self-sustained oscillator originates from the interplay between TO and FCD mechanisms, forcing the resonance to oscillate around λ_l at a frequency of ν_{SP}, and consequently affecting the number of photons entering the cavity. In that regard, the transmitted signal shows a periodic anharmonic variation over time (FIG. 3b) arising from the difference in the rates of temperature increase due to free-carrier recombination ($\tau_{FC} \sim$ ns) and heat dissipated to the surroundings of the structure ($\tau_T \sim \mu$s). The time required for a cycle to be completed is $1/\nu_{SP}$, depending on the dynamic processes involved. Specifically, when the cavity is progressively heated as λ_l increases, it results in a shorter cooling time and therefore a higher SP frequency [5]. This wide tunability of ν_{SP} is regarded as an advantage since it can be used for optical pumping of the phononic modes of the structure, as explained hereafter. Moreover, due to the anharmonic modulation of n, the signature of the SP limit cycle appears as a combination of several frequency harmonics embedded in the transmitted signal, located at integers of ν_{SP} ($M\nu_{SP}$) and whose intensity decreases with frequency. Meanwhile, the radiation pressure force inside the cavity ($F_0 = \hbar g_{OM} n$) is modulated likewise since it linearly depends on n, thus acting on the mechanical motion of the structure.

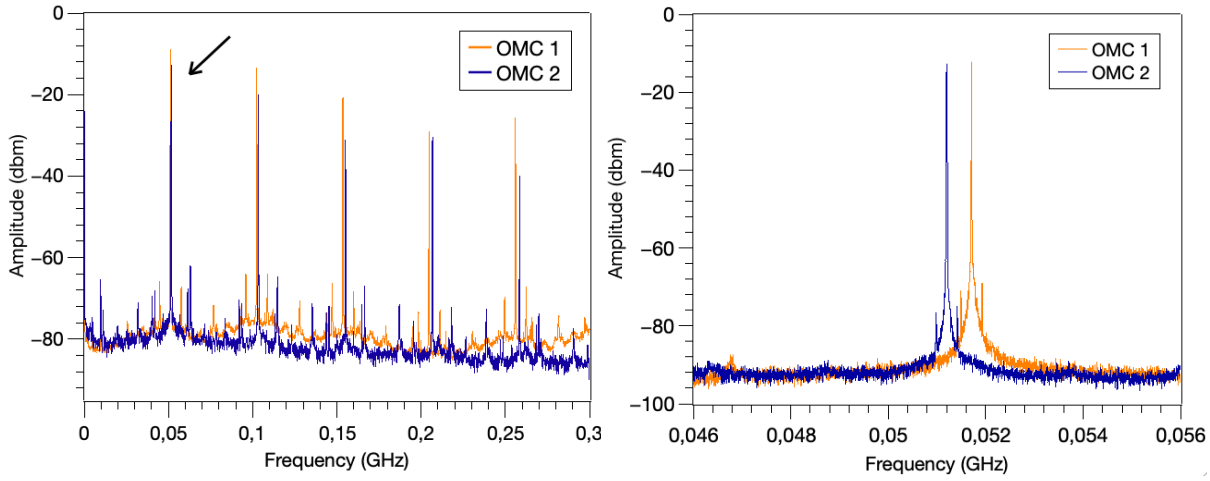

(a) (b)

Figure 4: (a) RF spectrum at phonon lasing regime when the 51MHz modes are locked at $M = 1$ of the SP. (b) Zoom-in of the first harmonic of the RF signal for lasing mechanical modes at 51.2 MHz and 51.7 MHz.

2.2. SP/Phonon lasing regime

Below the threshold imposed by the beginning of the self-pulsing regime, the RF spectrum only displays peaks of thermally driven low-frequency modes activated at room atmospheric conditions, previously reported in FIG. 2b. Furthermore, a previous work [6] indicates that once the SP regime is active and by further increasing λ_{I}, a new situation can emerge when one of the harmonics linewidth intersects with a transduced vibrational peak with sufficiently large g_{OM} ($M\nu_{\mathrm{SP}} = \Omega_M$). Said resonance is characterized by a high-amplitude and coherent state of the mechanical mode referred to as phonon lasing (FIG. 4a). In order to solve the SP/phonon lasing coupled dynamics, a 4D nonlinear system must be considered $\{\Delta$T, N, u, $\dot{u}\}$ due to the presence of the differential equation for the generalized coordinate for the displacement of a mechanical mode (u) [6]:

$$m_{\mathrm{eff}}\ddot{u} + m_{\mathrm{eff}}\frac{\Omega_m}{\Omega_{m,i}}\dot{u} + k_{\mathrm{eff}}u = F_0 \tag{4}$$

which corresponds to a damped linear harmonic oscillator driven by F_0 where m_{eff} is the mode's effective mass, k_{eff} is the mode's spring constant, and Ω_m is its eigenfrequency. In this context, the OMC mechanical oscillations provide an effective feedback, stabilizing and locking the self-pulsing frequency at: $\nu_{SP} = \Omega_m/M$. In other words, the two oscillators are frequency-entrained such that the SP adapts its oscillation frequency to be a fraction of the mechanical eigenfrequency.

3. Synchronization of OMCs

This experiment attempts to synchronize the OMCs characterized in the preceding section while both exhibit phonon lasing dynamics. Importantly, the frequency locking process takes place when both oscillators, each at its own frequency, begin to oscillate at the same frequency in response to a weak interaction between them.

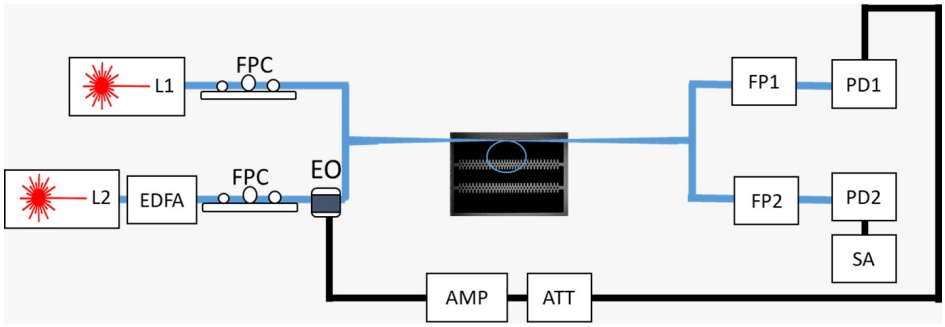

Figure 5: Experimental setup diagram involving the devices described in the document: tunable lasers (L1 and L2), an Erbium-Doped Fiber Amplifier (EDFA) to amplify L2's signal, polarization controllers (FPC), an electro-optic modulator (EO), a voltage-controlled amplifier (AMP, ATT), Fabry-Perot filters (FP), photodetectors (PD) and a spectrum analyzer (SA).

FIG. 4a illustrates the RF spectrum of both isolated structures during the phonon lasing regime. We took the ∼51MHz modes (marked in the figure) to perform the synchronization since they present the largest Q-factors and can be effectively coupled to the lower SP harmonics which display the strongest intensity. To ensure an effective process, the frequency detuning should be small, i.e., the mechanical modes under consideration must be close together (FIG. 4b). Furthermore, the interaction between both systems is governed by a Master-Slave configuration. An arrangement of this kind comprises a driven (Slave) system that adapts its dynamics to a driving (Master) system. The interaction is achieved by reproducing the optical signal modulation of the Master output, which carries the information of the Master mechanical position, to the Slave input signal. The coupling strength is intensified using a voltage-controlled variable-gain amplifier on the Master OMC signal.

3.1. Experimental setup and results

The procedure to obtain frequency locking involves the following steps according to the setup in FIG. 5. Firstly, two tunable lasers simultaneously excite the first cavities' resonance at ∼1523nm and ∼1530nm, respectively. Secondly, nonlinear dynamics described in Section 2 are observed as the laser's wavelength is increased, ultimately generating mechanical lasing at the ∼51 MHz modes by locking them with the first harmonic (M=1) of the self-pulsing. At this point, we assign each oscillator either a Master or a Slave role, so that L1 will address the Master OMC and L2 the Slave OMC. It is worth noting that the role of the OMCs can be exchanged by just switching the laser wavelengths. Then, there is a split of the output transmission carrying the signal embedding both OMC dynamics into two channels. In the first path, a Fabry-Perot filter (FP) isolates the signal coming from the assigned Master OMC before being transferred to the first photodetector (PD1). The optical signal obtained from the driving oscillator containing information about its mechanical dynamics is amplified or attenuated (AMP/ATT) using a voltage-controlled amplifier and then connected to the electro-optic modulator (EOM) placed at the input of the Slave. Therefore, the AMP/ATT stage controls the interaction strength between the two OMC oscillators in an unidirectional

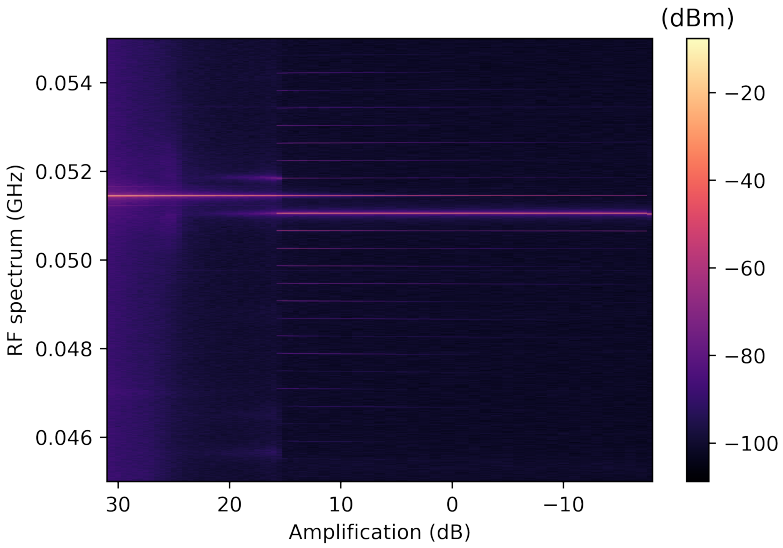

Figure 6: OMC 1 (51.4 MHz) performs as Master and OMC 2 (51.03 MHz) as Slave. Evolution of RF spectrum as a function of the gain corresponding to a backward scanning where the Slave returns to its natural frequency by decreasing the gain of the Master signal.

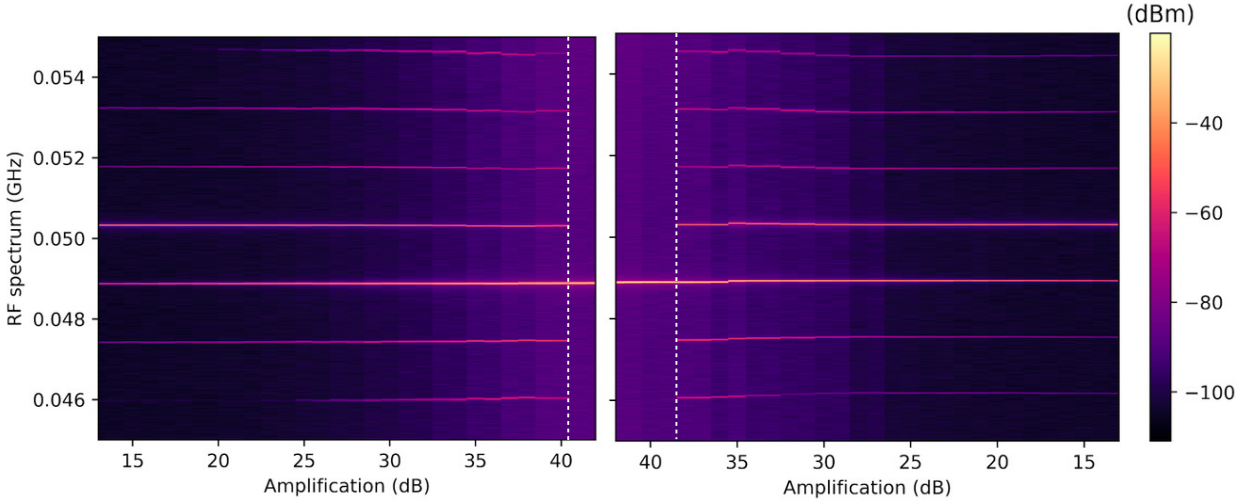

(a) (b)

Figure 7: OMC 2 (49 MHz) performs as Master and OMC 1 (50.5 MHz) as Slave. Evolution of the RF spectrum as a function of the gain corresponding to a forward (a) and backward (b) scanning where the Slave is locked to the Master frequency (dashed line) by increasing the gain and then returned to its natural frequency (dashed line).

way. In the second path, the driven OMC signal is isolated by another FP and passes through the second photodetector (PD2), finally reaching the spectrum analyzer to display the RF spectrum embedded in the Slave output.

Since the sample is prone to change characteristics with minimal environmental changes, the alignment conditions must be extremely accurate to effectively couple light into the cavity and thus reach all regimes. Even so, temperature changes and usually the alignment conditions slightly shift the OMCs mechanical frequencies at each experiment.

A gain of 31 dB is initially applied in the AMP/ATT stage to the driving OMC signal using a configuration in which OMC 1 is the Master. FIG. 6 shows the set of RF spectra obtained by decreasing the AMP/ATT values from 31dB down to -18dB. The backward scanning demonstrates that from 31dB to 15 dB, the Slave is locked at the Master frequency (51.4 MHz). Below the latter value, there is a change of dynamics in which the Slave OMC returns to its natural frequency. Several sidebands are also visible at low coupling strength, reflecting the many combinations of the two sinusoidal mechanical modes' sum laying close together. An illustration of the experiment in a configuration in which we have inverted the role of the OMCs (now OMC 2 acts as Master and OMC 1 as Slave) is provided in FIG. 7. During forward scanning i.e., increasing the gain values, a relatively high gain (41 dB) causes the driven frequency to abruptly switch from its natural position to the Master frequency. As shown in backward scanning, a slight amount of hysteresis is apparent in both configurations, given that the Slave returns to oscillate with its own natural frequency at a different gain value.

It cannot be ruled out that we only demonstrated frequency locking between two mechanical oscillators in the frequency domain, similarly done in past literature [1] using another kind of OM oscillator. Yet further data is needed to prove whether the coupling between both OMCs is correctly achieved. In this account, we analyzed the temporal response of the Master transmission after being amplified at low and high gain, observing significant differences in the modulation between both signals. FIG.8a shows the response at low amplification resembling the Master signal in FIG.3b, while at high amplification, FIG.8b presents an altered modulation. The latter effect is due to the performance of the amplifier, which ceases to operate at its linear range when the voltage applied is too high, thus causing the signal to perturb its modulation. Consequently, the synchronization takes longer, as the signal used to modulate the Slave does not exactly match the Master RF oscillations, only a signal of the same frequency (ν_{SP}).

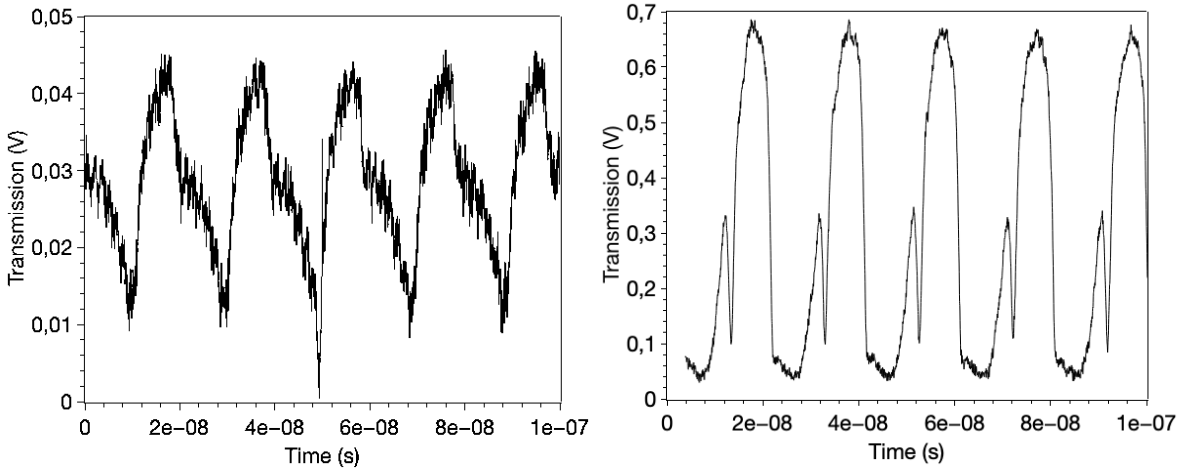

(a) (b)

Figure 8: Transmitted Master signal at the output of the amplifier when applying a (a) low gain ($\sim$13 dB) and (b) a high gain ($\sim$38 dB.)

4. Conclusions

In this study, we outlined some possible applications of the OMCs and performed their experimental characterization, which led us to introduce a general view of the nonlinear dynamics involving these kinds of structures. With light as a mechanism of interaction, we also found a way to achieve frequency locking between two OM oscillators when both display phonon lasing dynamics using either OMC as a driving oscillator. However, the experiment only examined this process within the frequency domain, which does not confirm whether the coupling between both OMCs was successfully realized. Indeed, it was detected the Master dynamics were not entirely transferred to the Slave since the signal modulation coupling both OMCs was perturbed as we increased the coupling strength intensity. A possible way to overcome this issue for further research involves using a new set of OMCs with fewer fabrication imperfections. By improving the samples, their mechanical modes can manifest substantially closer to one another, requiring less voltage to achieve synchronization and thus allowing a linear amplification of the coupling strength, which leads to a faster and more efficient process.

Acknowledgments

I'm extremely grateful to my advisor, Prof. Daniel Navarro for his invaluable patience, feedback, and support during the course of the project. His tutelage and advice have helped me improve both my lab and academic skills. My appreciation also goes out to my partner, family, and friends for their encouragement all through my studies. Finally, I would like to thank the University of Barcelona for providing such an equipped laboratory to conduct my study.

5. References

[1] Shah, S. Y., Zhang, M., Rand, R., & Lipson, M. (2015). Master-slave locking of optomechanical oscillators over a long distance. Physical review letters, 114(11), 113602.

[2] Oudich, M., El-Jallal, S., Pennec, Y., Djafari-Rouhani, B., Gomis-Bresco, J., Navarro-Urrios, D., ... & Makhoute, A. (2014). Optomechanic interaction in a corrugated phoxonic nanobeam cavity. Physical Review B, 89(24), 245122.

[3] Aspelmeyer M., Kippenberg T.J. and Marquardt F., 2014, Cavity Optomechanics, Reviews of Modern Physics, 86,1391

[4] Navarro-Urrios, D., Capuj, N. E., Gomis-Bresco, J., Alzina, F., Pitanti, A., Griol, A., ... & Torres, S. (2015). A self-stabilized coherent phonon source driven by optical forces. Scientific reports, 5(1), 1-7.

[5] Maire, J., Arregui, G., Capuj, N. E., Colombano, M. F., Griol, A., Martinez, A., ... & Navarro-Urrios, D. (2018). Optical modulation of coherent phonon emission in optomechanical cavities. APL Photonics, 3(12), 126102.

[6] Navarro-Urrios, D., Capuj, N. E., Colombano, M. F., García, P. D., Sledzinska, M., Alzina, F., ... & Sotomayor-Torres, C. M. (2017). Nonlinear dynamics and chaos in an optomechanical beam. Nature communications, 8(1), 1-10.